This is a post-peer-review, pre-copyedit version of an article published in IEEE TRANSACTIONS ON ANTENNAS AND PROPAGATION. The final authenticated version is available online at: https://doi.org/10.1109/TAP.2017.2700044

Comprehensive Comparison of Compact UWB Antenna Performance by Means of Multiobjective Optimization

Slawomir Koziel, *Senior Member, IEEE*, and Adrian Bekasiewicz

***Abstract*— An optimization-based procedure for comprehensive performance comparison of alternative compact UWB antenna topologies is discussed. The assessment of the antenna performance is conducted with respect to the structure size and its reflection response. More specifically, the best possible tradeoffs between these two figures of merit are identified through multiobjective optimization at the level of full-wave electromagnetic (EM) simulation. Analysis of Pareto-optimal designs obtained for various antenna topologies allow for their fair comparison; particularly in terms of the minimum size, they can be designed for (assuming acceptable reflection response levels) or the best attainable reflection characteristics. For the sake of computational efficiency, the multiobjective optimization algorithm utilized in this paper exploits sequential domain patching technique and variable-fidelity EM simulation models, which is a fully automated procedure that permits finding Pareto set representations at the cost corresponding to about a hundred of high-fidelity EM analyses of a given structure. The proposed approach is demonstrated using three topologies of compact UWB-monopole antennas. Comparison of antenna with respect to three objectives (also including total efficiency) is also discussed. Simulation results are verified using experimental data.**

***Index Terms*— Antenna design, design optimization, multiobjective optimization, performance comparison, simulation-driven design, surrogate modeling, UWB antennas.**

I. Introduction

SIZE reduction has become an important criterion in the design of contemporary UWB antennas. Miniaturization can be critical for some applications, such as handheld or wearable devices [1]–[4], or, recently, the growing area of the Internet of Things [5], [6]. Unfortunately, reduction of the antenna footprint is normally in conflict with achieving acceptable electrical performance. The fundamental physical reason is that shortening of the current path resulting from structure reduction [7]–[10] leads to degradation of the antenna matching at lower frequencies.

Manuscript received May 19, 2016; revised January 30, 2017; accepted April 22, 2017. Date of publication May 2, 2017; date of current version July 1, 2017. This work was supported in part by the Icelandic Centre for Research under Grant 174114051 and in part by the National Science Centre of Poland under Grant 2015/17/B/ST6/01857. *(Corresponding author: Slawomir Koziel.)*

The authors are with the School of Science and Engineering, Reykjavik University, 101 Reykjavik, Iceland, and also with the Faculty of Electronics, Telecommunications and Informatics, Gdansk University of Technology, Gdansk, Poland (e-mail: koziel@ru.is; bekasiewicz@ru.is).

Color versions of one or more of the figures in this paper are available online at http://ieeexplore.ieee.org.

Digital Object Identifier 10.1109/TAP.2017.2700044

Numerous methods have been proposed over the last years to address the problem of UWB antenna minimization. The most popular techniques include various ground plane modifications of monopole-based topologies (e.g., I-shaped, L-shaped, or meandered stubs [11], [12], structures with enhanced ground plane [13], or slits below the microstrip line [11], [12]), uniplanar geometries [10], [14], [15], quasi self-complementary topologies [16]–[18], or slot antennas [8], [19], [20]. The aforementioned modifications often allow for considerable reduction of the antenna size. At the same time, they result in the increased complexity of the antenna topology as well as additional geometry parameters that need to be adjusted. Consequently, the design process of compact UWB antennas becomes quite challenging, because full-wave electromagnetic (EM) analysis needs to be used for reliable performance evaluation. Moreover, due to a small antenna size, inclusion of the environmental components (such as connectors) into the EM model is mandatory which further increases the evaluation cost.

Due to the lack of design-ready theoretical models for compact UWB antennas, EM-driven design closure (in the sense of adjustment of antenna dimensions) is a necessity. As a result of the difficulties mentioned before, commonly used simulation-based approaches are hands-on methods exploiting parameter sweeps guided by engineering experience [1], [18], [19]. Such methods are laborious due to heavy supervision required from the designer, yet, may lead to acceptable results within reasonable timeframe. However, they are unable of yielding truly optimum designs. These can only be obtained by simultaneous adjustment of all relevant parameters using automated numerical optimization [8], [10], [12]. The latter is often computationally prohibitive when using conventional algorithms [21], [22]. Design speedup can be achieved using surrogate-assisted methods [23]–[26] as well as adjoint sensitivities [27]–[29] (the latter used to improve efficiency of gradient-based optimization [29]). Neither of these approaches are yet widespread in the antenna community.

Difficulties in proper dimension optimization lead to the situation where the compact UWB antenna designs reported in the literature are far from being optimum [30], [31]. Consequently, their comparisons in terms of either size or electrical performance are not quite meaningful. In particular, given two or more compact UWB antenna structures, it may not be conclusive to say which one outperforms the others (with respect to the size or other performance figures), based on

the results reported in the literature, just because the specific designs given are usually far from being optimum.

In this paper, we propose a comprehensive approach to assessment of compact UWB antenna structures by means of their rapid multiobjective optimization and comparison of the corresponding sets of Pareto-optimal designs representing the best possible tradeoffs between conflicting design criteria, here, the antenna footprint and its reflection characteristic (such as the maximum in-band reflection level). A Pareto set provides the most comprehensive information including such data as the minimum attainable footprint that still ensures acceptable in-band reflection or the best attainable reflection level. In order to yield Pareto sets at low computational cost, we exploit a sequential domain patching (SDP) algorithm [32], which is a deterministic (nonevolutionary) and fast multiobjective optimization method involving variable-fidelity EM simulation models and response correction techniques. Side-by-side comparison of the Pareto sets corresponding to various antenna structures allows for fair assessment of their capabilities, in particular, the minimum attainable size (while maintaining acceptable reflection levels). Our approach is demonstrated using three structures of compact UWB-monopole antennas. Selected designs have been fabricated and measured in order to provide additional validation of the simulation results. As a step toward even more comprehensive antenna treatment, a case study of three-objective comparison has been considered that involves total efficiency as a design criterion (in addition to the antenna size and reflection characteristic).

II. Antenna Performance Comparison Using Pareto Sets

The two most important types of figures of merit that are subjected to optimization process are electrical performance and the antenna size. Electrical performance parameters include antenna matching, efficiency, radiation pattern stability, phase center stability, etc. Here, for the sake of example, reflection response is considered as an electrical performance parameter so that the antenna comparison is executed with respect to two objectives (see Section V for an example of three-objective comparison).

In most cases, reflection response is optimized directly in order to ensure acceptable antenna performance whereas small size is normally a result of the introduced geometry modifications [7], [13], [31]. Some methods for explicit minimization of the antenna size have also been recently reported [10], [12]. Regardless of the formulation of the design problem, usually a single design is produced as the outcome of the optimization algorithm.

More comprehensive information about capabilities of a given antenna, e.g., in terms of the best possible trade-offs between the structure size and the maximum in-band reflection, can be obtained by means of multiobjective optimization [32]–[34]. In practice, this information is obtained in the form of a discrete set (the so-called Pareto set) of alternative designs [32], [35] as shown in Fig. 1. Conclusive assessment of two or more antenna structures can be realized by comparing their corresponding Pareto sets. This is illustrated in Fig. 2

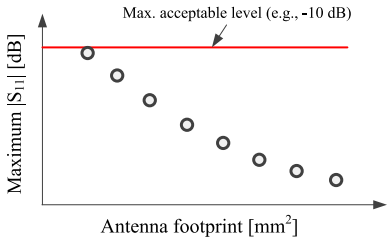

Fig. 1. Conceptual illustration of the Pareto set for a compact UWB antenna with the two design objectives being minimization of the maximum in-band antenna reflection and minimization of the antenna footprint.

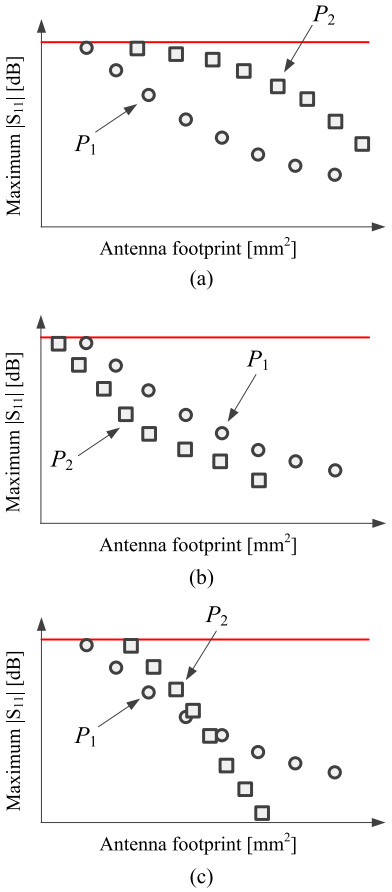

Fig. 2. Comparison of antenna structures A_1 and A_2 based on their Pareto sets P_1 and P_2. Some of possible scenarios. (a) Complete domination of P_1 over P_2. (b) Complete domination of P_2 over P_1. (c) Partial domination of P_1 over P_2.

which shows some of the possible scenarios concerning Pareto set allocation. Domination of one of the Pareto sets over the other indicates that the corresponding antenna structure outperforms its competitor in both aspects taken into account (size and reflection response). Partial domination indicates that one of the antennas exhibits better miniaturization potential, whereas the other can be designed for superior electrical performance. The knowledge of the Pareto set also allows for selecting a design that ensures a specific maximum in-band reflection level (e.g., −12 dB) that might be important (as a safety margin) to account for possible manufacturing tolerances.

A practical problem is that multiobjective optimization of antennas is a very challenging task when EM analysis is used for structure evaluation [36], [37]. Utilization of EM-simulation models is mandatory in case of compact antennas. Furthermore, the models have to incorporate connectors (and other relevant environmental components) [8], [10], [38]. This increases computational complexity of EM analysis but is mandatory to ensure accuracy.

The most popular multiobjective optimization methods, i.e., population-based metaheuristics are of limited use because of their tremendous computational cost. Recently, several surrogate-assisted techniques have been developed for low-cost multiobjective antenna design [32], [39], [40]. Their key components are utilization of variable-fidelity EM simulations [41], as well as auxiliary response surface approximation (RSA) models [42] but also initial design space reduction [43]. One of these methods, SDP [32], is exploited in this work to execute Pareto set identification and subsequent antenna comparison. Its advantage over the earlier techniques [39], [40], [43] is that it employs neither evolutionary algorithms (at any stage of the design process) nor RSA models. It is, therefore, easy to implement, automated, and fully deterministic.

III. Fast Multiobjective Optimization Using Domain Patching

As mentioned in Section II, identification of Pareto sets for the considered compact UWB antennas will be realized using the SDP algorithm [32]. Below, we give a brief outline of SDP.

A. Multiobjective Optimization Problem Formulation

Let $\boldsymbol{R}_f(\boldsymbol{x})$ denotes a response of an accurate EM antenna model with $\boldsymbol{x}$ being a vector of design variables. Let $F_k(\boldsymbol{R}_f(\boldsymbol{x}))$, $k = 1, \ldots, N_{\text{obj}}$, be a kth design objective. If $N_{\text{obj}} > 1$, the solutions are compared using the dominance relation [35] defined as: $\boldsymbol{y} \prec \boldsymbol{x}$($\boldsymbol{y}$ dominates over $\boldsymbol{x}$) if $F_k(\boldsymbol{R}_f(\boldsymbol{y})) \leq F_k(\boldsymbol{R}_f(\boldsymbol{x}))$ for all $k = 1, \ldots, N_{\text{obj}}$, and $F_k(\boldsymbol{R}_f(\boldsymbol{y})) < F_k(\boldsymbol{R}_f(\boldsymbol{x}))$ for at least one k. We aim at finding a representation of a so-called Pareto set X_P of nondominated designs so that for any $\boldsymbol{x} \in X_P$ there is no $\boldsymbol{y}$ for which $\boldsymbol{y} \prec \boldsymbol{x}$ [35]. An example of the Pareto set is shown in Fig. 1. As explained in Section II, Pareto-optimal designs represent the best possible tradeoffs between conflicting objectives.

B. Sequential Domain Patching Algorithm

The SDP algorithm is initialized from the "extreme" points of the Pareto front found by solving single-objective problems

$$\boldsymbol{x}_k^* = \arg\min_{\boldsymbol{x}} F_k(\boldsymbol{R}_c(\boldsymbol{x})) \tag{1}$$

for $k = 1, \ldots, N_{\text{obj}}$ [43]. In order to reduce the computational cost, the problem (1) is solved at the level of a coarse-discretization (low-fidelity) EM model $\boldsymbol{R}_c$.

The initial representation of the Pareto set is found using the procedure outlined below where n stands for the number of design variables. Here, $N_{\text{obj}} = 2$ is assumed, which is the most typical situation (e.g., antenna size versus electrical performance such as the maximum in-band reflection level).

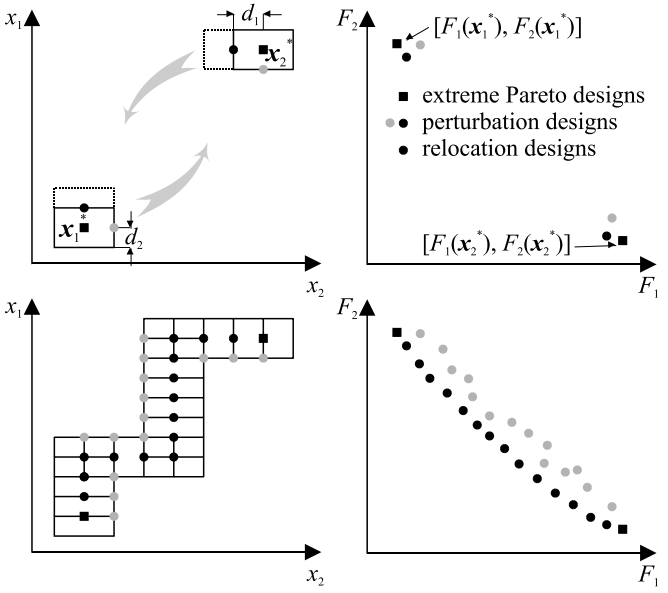

Fig. 3. Conceptual illustration of the SDP algorithm. The routine is terminated after closing the path between the extreme designs.

The SDP algorithm flow [32] as follows.

1) Set the patch size $\boldsymbol{d} = [d_1 \ldots d_n]^T$ (see Section III-C).
2) Set the current points $\boldsymbol{x}_{c1} = \boldsymbol{x}_1^*$ and $\boldsymbol{x}_{c2} = \boldsymbol{x}_2^*$.
3) Evaluate n perturbations of the size $\boldsymbol{d}$ around $\boldsymbol{x}_{c1}^*$ (toward $\boldsymbol{x}_{c2}^*$) and select the best with respect to F_2.
4) Center the patch at the point selected in Step 3; update $\boldsymbol{x}_{c1}$.
5) Evaluate n perturbations of the size $\boldsymbol{d}$ around $\boldsymbol{x}_{c2}^*$ (toward $\boldsymbol{x}_{c1}^*$) and select the best with respect to F_1.
6) Center the patch at the point selected in Step 5; update $\boldsymbol{x}_{c2}$.
7) If the path is not complete, go to 3.

The algorithm operation is illustrated in Fig. 3. The SDP procedure produces the initial representation of the Pareto set. The computational cost of the algorithm depends on the design space dimensionality n and on the total number of patches. Therefore, its upper bound can be estimated as $(M-1)\cdot(n-1)$, where $M = \sum_{k=1,\ldots,n} m_k$, and m_k is the number of intervals in the direction j. In practice, only the perturbations toward opposite extreme Pareto designs are evaluated, and thus, the overall cost is normally lower than the estimation.

C. Patch Size Determination

The distance between the extreme Pareto-optimal solutions $\boldsymbol{x}_1^*$ and $\boldsymbol{x}_2^*$ is split into integer-valued number of intervals. The number of intervals in each direction is selected to ensure that the change (e.g., norm wise) of the antenna responses is similar when making patch-size perturbations with respect to each direction. In other words, the number of patches is larger for more sensitive geometry parameters.

In the following, we use the notation $\boldsymbol{x}_1^* = [x_{1.1}^* \ldots x_{1.n}^*]^T$ and $\boldsymbol{x}_2^* = [x_{2.1}^* \ldots x_{2.n}^*]^T$ to identify components of the extreme points $\boldsymbol{x}_1^*$ and $\boldsymbol{x}_2^*$. The numbers m_k are assigned as follows.

We start by evaluating $\boldsymbol{R}_c$ at n points $\boldsymbol{x}_{1-2}^{(k)} = [x_{1.1}^* \ldots x_{1.k-1}^* x_{2.k}^* x_{1.k+1}^* \ldots x_{1.n}^*]^T$, $k = 1, \ldots, n$. Subsequently, one calculates $E_{1.k} = ||\boldsymbol{R}_c(\boldsymbol{x}_{1-2}^{(k)}) - \boldsymbol{R}_c(\boldsymbol{x}_1^*)||/||\boldsymbol{R}_c(\boldsymbol{x}_1^*)||$, $k = 1, \ldots, n$. In the same way, we evaluate $\boldsymbol{R}_c$ at $\boldsymbol{x}_{2-1}^{(k)} = [x_{2.1}^* \ldots x_{2.k-1}^* x_{1.k}^* x_{2.k+1}^* \ldots x_{2.n}^*]^T$, $k = 1, \ldots, n$, and calculate $E_{2.k} = ||\boldsymbol{R}_c(\boldsymbol{x}_{2-1}^{(k)}) - \boldsymbol{R}_c(\boldsymbol{x}_2^*)||/||\boldsymbol{R}_c(\boldsymbol{x}_2^*)||$, $k = 1, \ldots, n$. Finally, we set $m_k = \max\{2, \lceil m_{\max} \cdot E_k \rceil\}$, $k = 1, \ldots, n$, where $E_k = E_{0k}/\max\{E_{0j}\colon j = 1, \ldots, n\}$, and $E_{0k} = (E_{1.k} + E_{2.k})/2$.

The factors $E_{1.k}$ determine the relative response changes when varying the kth components of the design $\boldsymbol{x}_1^*$ toward $\boldsymbol{x}_2^*$ (similarly for $E_{2.k}$). They give an idea of how much the antenna responses change when moving from one extreme Pareto point to another along a specific geometry dimension. The factors E_k are the average values. The number of intervals is proportional to E_k (the minimum number of intervals is set to 2; the numbers are rounded up to the nearest integer).

D. Pareto Set Refinement

The initial approximation of the Pareto set generated by the SDP algorithm is obtained for the low-fidelity model $\boldsymbol{R}_c$. In order to find the high-fidelity Pareto-optimal designs, a subset of the selected designs $\boldsymbol{x}_c^{(k)}$, $k = 1, \ldots, K$, extracted from the initial set is refined as follows [32]:

$$\boldsymbol{x}_f^{(k)} \leftarrow \underset{\boldsymbol{x},\ F_2(\boldsymbol{x}) \le F_2\left(\boldsymbol{x}_f^{(k)}\right)}{\arg\min} F_1\left(\boldsymbol{R}_s(\boldsymbol{x}) + \left[\boldsymbol{R}_f\left(\boldsymbol{x}_f^{(k)}\right) - \boldsymbol{R}_s\left(\boldsymbol{x}_f^{(k)}\right)\right]\right). \tag{2}$$

The process (2) improves the first objective without degrading the second one. The starting point for (2) is $\boldsymbol{x}_f^{(k)} = \boldsymbol{x}_c^{(k}$, and the process is iterated until convergence. Usually, two iterations are sufficient. $\boldsymbol{R}_s$ is a second-order polynomial approximation (without mixed terms) [10] of the low-fidelity model $\boldsymbol{R}_c$ setup using the evaluation of $\boldsymbol{R}_c$ at $\boldsymbol{x}_c^{(k)}$ and the perturbed designs corresponding to the patch centered around $\boldsymbol{x}_c^{(k)}$. Because of good correlation between the low- and high-fidelity models, only two iterations of (2) are normally sufficient to find the refined design.

IV. Case Studies: UWB Monopoles

In this section, we consider three structures of compact UWB antennas recently proposed in the literature [30], [31], [44], and carry out their comprehensive comparison using the methodology of Sections II and III.

A. Antenna Structures

Fig. 4 shows geometries of the considered antennas. All structures are designed on a 0.762-mm-thick Taconic RF-35 dielectric substrate ($\varepsilon_r = 3.5$, $\tan\delta = 0.0018$). Antenna models are implemented in CST Microwave Studio and simulated using its time domain solver [45]. The first structure (Antenna I) consists of a circular patch fed through a tapered 50-Ω microstrip line and modified ground plane with L-shaped strip aimed at enhancement of the current path within the compact geometry [30]. The design variables are: $\boldsymbol{x}_{\rm I} = [w_0\ l_1\ l_2\ l_3\ l_4\ w_1\ w_2\ w_3\ r\ o_r]^T$, whereas parameters $w_f = 1.7$, $l_f = 10$, and $o = 0.5w_0 \cdot r \cdot o_r$ (all dimensions in mm). The high-fidelity antenna model $\boldsymbol{R}_f$ consists of ∼2 600 000 mesh cells (simulation time 24 min). The low-fidelity model $\boldsymbol{R}_c$ contains ∼370 000 cells (simulation time 150 s). The models include the SMA connector to ensure reliability of antenna evaluation. The ranges of design variables for considered design are: $\boldsymbol{l}_{\rm I} = [15\ 2\ -2\ 10\ 3\ 0.2\ 0.2\ 0.2\ 4.5\ -1]^T$ and $\boldsymbol{u}_{\rm I} = [30\ 8\ 2\ 15\ 8\ 1.7\ 1.2\ 1.2\ 8.5\ 1]^T$.

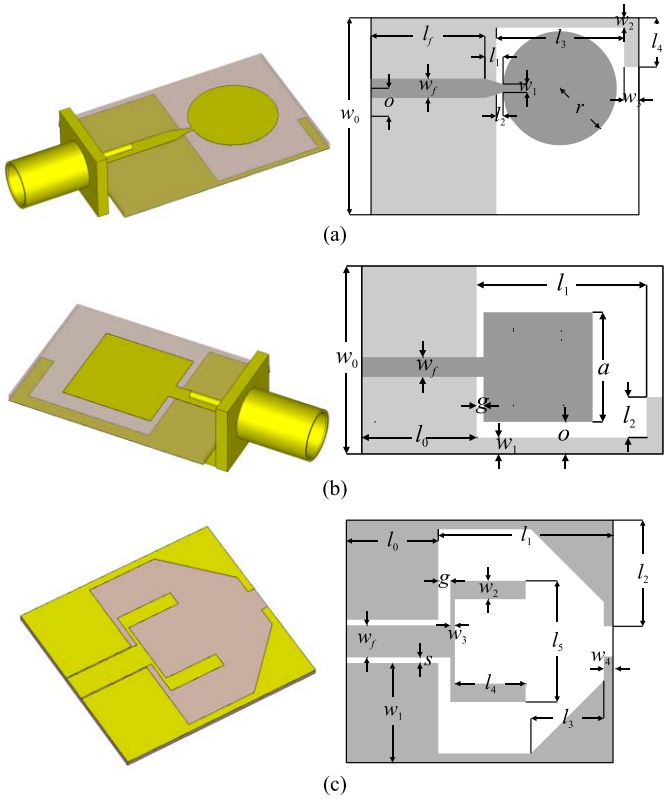

Fig. 4. Geometries of UWB antennas considered in our comparative study. (a) Antenna I [30]. (b) Antenna II [44]. (c) Antenna III [31].

The second structure (Antenna II) consists of a rectangular radiator and a ground plane with L-shaped strip for current path enhancement [44]. The structure is a simplified version of a single radiator extracted from the MIMO antenna proposed in [7]. The vector of design variables is $\boldsymbol{x}_{\rm II} = [l_0\ g\ al_1\ l_2\ w_1 o]^T$. Parameter $w_0 = 2o+a$, whereas the feeding linewidth $w_f = 1.7$ mm to ensure 50-Ω input impedance. The unit for all dimensions is mm. The EM antenna models are implemented in CST Microwave Studio ($\boldsymbol{R}_f$: ∼4 600 000 mesh cells, simulation time 40 min, and $\boldsymbol{R}_c$: ∼850 000 cells, 2 min). Similarly as for Antenna I, the models include the SMA connector to ensure reliability of antenna evaluation. The ranges of design variables for considered design are: $\boldsymbol{l}_{\rm II} = [4\ -2\ 4\ 5\ 1\ 0.5\ 0.5]^T$ and $\boldsymbol{u}_{\rm II} = [15\ 2\ 15\ 20\ 10\ 3.5\ 5.5]^T$.

The third design (Antenna III) is a uniplanar structure composed of a driven element in the form of fork-shaped radiator fed through a coplanar waveguide. Also the structure has an open-slot geometry [31]. The design variables are: $\boldsymbol{x}_{\rm III} = [l_0\ l_1\ l_{2r}\ l_{3r}\ l_4\ l_5\ w_1\ w_2\ w_3\ w_4\ g]^T$. Parameters $w_f = 3.5$ and $s = 0.16$, whereas variables $l_2 = (0.5w_f + s + w_1) \cdot \max\{l_{2r}, l_{3r}\}$ and $l_3 = (0.5w_f + s + w_1) \cdot l_{3r}$.

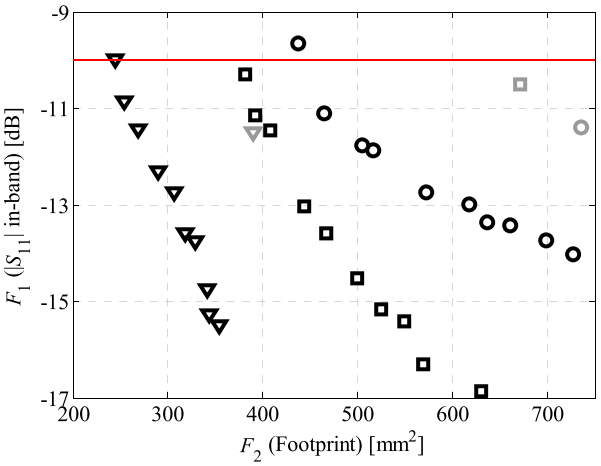

Fig. 5. Comparison of the high-fidelity Pareto sets for Antenna I (□), Antenna II (∇), and Antenna III (○). Gray symbols denote designs of the considered antennas obtained based on the literature. Note that, for each case, they are dominated by the respective Pareto sets.

The low-fidelity antenna model consists of ∼215 000 cells (simulation time 67 s), whereas the high-fidelity one is composed of ∼1 600 000 cells (simulation time 10 min). The ranges of design parameters are: $\boldsymbol{l}_{\rm III} = [5\ 15\ 0.2\ 0.2\ 4\ 8\ 7\ 0.5\ 0.2\ 0.2\ 0.2]^T$ and $\boldsymbol{u}_{\rm III} = [15\ 25\ 1\ 0.8\ 11\ 16\ 15\ 3.5\ 2.5\ 2\ 2]^T$.

Based on the structure dimensions from [7], [30], and [31] one can conclude that Antenna III is noticeable larger (766 mm^2) than Antenna I (673 mm^2). At the same time, the footprint of the Antenna II is only 390 mm^2.

The following two design objectives are considered to compare the designs: F_1—minimization of reflection in 3.1- to 10.6-GHz band and F_2—minimization of footprint. The latter is defined as $A_I(\boldsymbol{x}_{\rm I}) = w_0 \cdot \max\{l_f + l_1 + 2r - 0.05r, l_f + l_1 - 0.05r + l_2 + l_3 + w_3\}$, $A_{\rm II}(\boldsymbol{x}_{\rm II}) = (a + 2o)(l_0 + l_1 + w_1)$, and $A_{\rm III}(\boldsymbol{x}_{\rm III}) = (l_0 + l_1) \cdot (2s + 2w_1 + w_f)$ for Antennas I–III, respectively. It should be noted that only the antenna responses for which in-band reflection is below −10 dB level are considered acceptable.

B. Pareto Set Identification Using SDP

Fig. 5 shows the Pareto fronts obtained using the SDP algorithm for the three antenna structures considered. Fig. 6 shows their reflection characteristics for the selected Pareto-optimal designs. Corresponding dimensions have been gathered in Tables I–III for the Antennas I, II, and III, respectively. The computational cost of the multiobjective optimization process is low and corresponds to only 128 high-fidelity model simulations for Antenna I (including 944 evaluations of $\boldsymbol{R}_c$ and 30 evaluations of $\boldsymbol{R}_f$). The cost for Antenna II corresponds to 72 evaluations of the high-fidelity model (831 × $\boldsymbol{R}_c$ and 30 × $\boldsymbol{R}_f$). Finally, the cost for Antenna III corresponds to 132 evaluations of the high-fidelity model (914 × $\boldsymbol{R}_c$ and 30 × $\boldsymbol{R}_f$). Note that the costs are similar for all structures.

The computational costs of the SDP algorithm obtained for Antennas I and II have been compared with two benchmark techniques exploiting multiobjective evolutionary

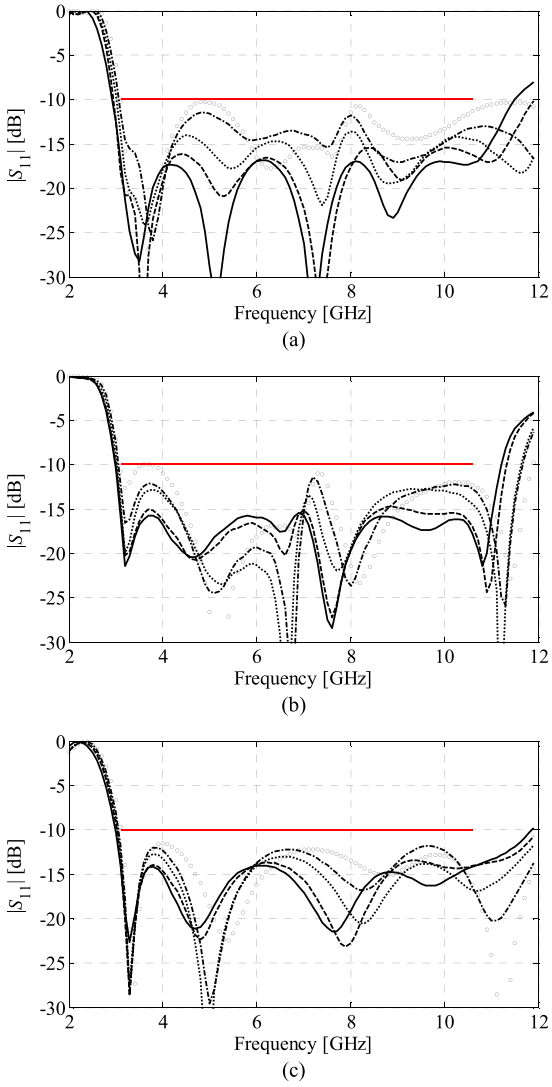

Fig. 6. Frequency responses of the high-fidelity model. (a) Antenna I for the designs listed in Table I. (b) Antenna II for the designs from Table II. (c) Antenna III for the designs from Table III. For all structures, the designs are as follows: $\boldsymbol{x}_f^{(1)}$—(—-), $\boldsymbol{x}_f^{(3)}$—(—-), $\boldsymbol{x}_f^{(6)}$—(· · ·), $\boldsymbol{x}_f^{(8)}$—(– ·), and $\boldsymbol{x}_f^{(10)}$—(○).

algorithm (MOEA) [35]. The MOEA-based optimizations have been performed within the search space regions defined in Section IV-A. In the first approach, MOEA has been executed on a kriging interpolation model constructed from low-fidelity model samples acquired within the region of interest (algorithm setup: population size: 1000, number of iterations: 50) [43]. In the second method, MOEA optimization is performed directly on the low-fidelity model $\boldsymbol{R}_c$ (setup: population size 100, number of iterations: 100). The reason for comparing the methods at the low-fidelity model level is an unacceptably high cost of MOEA optimization of the high-fidelity model $\boldsymbol{R}_f$ (estimated to be about ∼167 and ∼278 CPU-days for Antenna I and II, respectively).

For Antenna I, the numerical cost of SDP, kriging-based MOEA, and direct MOEA are 372 $\boldsymbol{R}_c$, 1402 $\boldsymbol{R}_c$, and 10 000 $\boldsymbol{R}_c$, respectively. Corresponding costs for Antenna II are 399 $\boldsymbol{R}_c$,

TABLE I

ANTENNA I: SELECTED PARETO-OPTIMAL DESIGNS

	F_1	F_2	Design Variables [mm]									
			w_0	l_1	l_2	l_3	l_4	w_1	w_2	w_3	r	o_r
$\boldsymbol{x}_f^{(1)}$	–16.9	630	22.24	4.36	–0.17	13.24	6.14	0.23	0.97	1.20	5.79	0.22
$\boldsymbol{x}_f^{(2)}$	–16.3	570	20.37	4.34	–0.11	12.94	5.86	0.21	0.57	1.07	5.54	0.36
$\boldsymbol{x}_f^{(3)}$	–15.4	549	20.24	4.14	–0.11	12.32	5.90	0.20	0.50	1.05	5.35	0.35
$\boldsymbol{x}_f^{(4)}$	–15.2	525	19.43	4.01	–0.09	12.32	5.86	0.20	0.49	1.05	5.28	0.39
$\boldsymbol{x}_f^{(5)}$	–14.5	500	18.49	4.01	–0.07	12.32	5.86	0.20	0.49	1.06	5.25	0.50
$\boldsymbol{x}_f^{(6)}$	–13.6	467	17.42	3.77	–0.04	12.32	6.00	0.22	0.48	1.03	5.18	0.60
$\boldsymbol{x}_f^{(7)}$	–13.0	443	16.61	3.60	–0.03	12.32	5.86	0.27	0.42	1.07	5.06	0.64
$\boldsymbol{x}_f^{(8)}$	–11.5	408	15.54	3.18	–0.03	12.32	5.86	0.24	0.42	1.01	4.95	0.63
$\boldsymbol{x}_f^{(9)}$	–11.2	392	15.54	2.44	–0.03	12.01	5.89	0.23	0.43	1.04	4.88	0.65
$\boldsymbol{x}_f^{(10)}$	–10.3	381	15.27	2.53	–0.13	11.81	6.01	0.20	0.52	1.02	4.92	0.64

TABLE II

ANTENNA II: SELECTED PARETO-OPTIMAL DESIGNS

	F_1	F_2	Design Variables [mm]						
			l_0	g	a	l_1	l_2	w_1	o
$\boldsymbol{x}_f^{(1)}$	–15.5	355	4.56	1.19	9.80	14.04	4.57	2.96	3.32
$\boldsymbol{x}_f^{(2)}$	–15.3	344	4.62	1.19	9.72	13.99	4.68	2.77	3.20
$\boldsymbol{x}_f^{(3)}$	–14.7	341	4.54	1.20	9.60	13.62	5.08	2.96	3.28
$\boldsymbol{x}_f^{(4)}$	–13.8	329	4.39	1.20	9.31	13.35	5.29	2.96	3.28
$\boldsymbol{x}_f^{(5)}$	–13.6	319	4.39	1.17	9.25	13.02	5.78	2.96	3.19
$\boldsymbol{x}_f^{(6)}$	–12.7	307	4.39	1.20	9.09	12.95	6.10	2.78	3.09
$\boldsymbol{x}_f^{(7)}$	–12.3	291	4.39	1.20	9.09	12.95	6.30	2.43	2.80
$\boldsymbol{x}_f^{(8)}$	–11.4	269	4.34	1.29	9.04	13.45	6.03	1.86	2.32
$\boldsymbol{x}_f^{(9)}$	–10.9	255	4.41	1.28	9.09	13.45	6.12	1.49	2.04
$\boldsymbol{x}_f^{(10)}$	–10.0	245	4.39	1.20	8.88	12.68	6.91	1.55	2.13

TABLE III

ANTENNA III: SELECTED PARETO-OPTIMAL DESIGNS

	F_1	F_2	Design Variables [mm]									
			l_0	l_1	l_{2r}	l_{3r}	l_4	l_5	w_1	w_2	w_3	w_4	g
$\boldsymbol{x}_f^{(1)}$	–14.0	727	9.04	18.3	0.89	0.61	8.40	14.7	11.4	2.89	0.49	1.46	0.52
$\boldsymbol{x}_f^{(2)}$	–13.7	698	9.04	18.0	0.88	0.58	8.53	14.6	11.0	2.91	0.45	1.31	0.49
$\boldsymbol{x}_f^{(3)}$	–13.4	661	9.04	17.5	0.90	0.69	8.31	14.6	10.5	2.86	0.42	1.04	0.48
$\boldsymbol{x}_f^{(4)}$	–13.4	637	8.98	17.5	0.86	0.67	8.35	14.6	10.1	2.74	0.48	0.90	0.50
$\boldsymbol{x}_f^{(5)}$	–13.0	618	8.95	17.5	0.91	0.72	8.22	14.6	9.78	2.91	0.42	0.82	0.48
$\boldsymbol{x}_f^{(6)}$	–12.7	573	8.76	17.5	0.82	0.76	8.34	14.5	9.00	2.91	0.42	0.61	0.46
$\boldsymbol{x}_f^{(7)}$	–11.9	517	9.04	16.9	0.91	0.68	8.53	14.7	8.08	2.91	0.43	0.38	0.45
$\boldsymbol{x}_f^{(8)}$	–11.8	505	9.02	16.6	0.87	0.77	8.13	14.5	7.95	2.91	0.42	0.35	0.45
$\boldsymbol{x}_f^{(9)}$	–11.1	465	8.78	16.5	0.84	0.82	8.13	14.3	7.29	2.63	0.52	0.25	0.40
$\boldsymbol{x}_f^{(10)}$	–9.6	438	7.80	16.7	0.71	0.83	8.17	14.5	7.02	2.91	0.52	0.22	0.44

1202 $\boldsymbol{R}_c$ and 10 000 $\boldsymbol{R}_c$. The results indicate that, for the considered antenna structures, the SDP approach is from 7 to 26 times faster compared to state-of-the-art multiobjective design approaches.

Fig. 6 shows the comparison of the Pareto sets obtained from both antennas. The discrepancies between the fronts along objective F_1 are below 2 dB which is minor from practical point of view. It should be noted that the Pareto set obtained by direct MOEA optimization of the $\boldsymbol{R}_c$ model is slightly dominated by the remaining ones which is due to terminating the algorithm after 10 000 model evaluations (necessary due to computational budget limitations, yet insufficient for convergence).

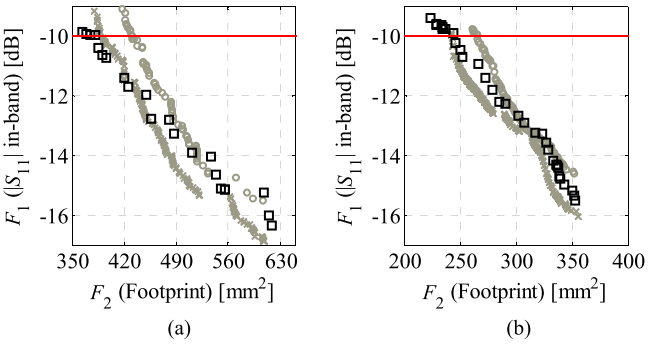

Fig. 7. Comparison of low-fidelity Pareto sets obtained using the SDP algorithm (□), MOEA optimization of the kriging model (×), and direct MOEA optimization of the low-fidelity model (○). (a) Antenna I. (b) Antenna II.

C. Structure Comparison

The results presented in Figs. 5 and 7 and Tables I–III indicate that Antenna I is entirely dominated by Antenna II, whereas Antenna III is dominated by Antenna I (consequently, Antenna II dominates over Antenna III as well) in the multiobjective sense. This means that Antenna I allows for achieving lower reflection level (around −17 dB in the UWB range for one of the extreme Pareto-optimal designs versus only about −14 dB for Antenna III), but it can also be designed for smaller size (381 mm^2 versus 438 mm^2 for Antenna III) while still maintaining acceptable level of −10 dB in-band reflection. At the same time, Antenna II exhibits the smallest footprint among the compared structures (only 245 mm^2 for the smallest design with acceptable reflection). Furthermore, it provides a broader range of changes along objective F_1 than Antenna III (5.6 dB versus 4.3 dB). Finally, for the in-band reflection level of −11 dB, the footprints of Antennas I–III are 392, 255, and 465 mm^2, respectively.

It should be noted that the largest design from the Pareto set obtained for Antenna II is characterized by in-band reflection of −15.5 dB and the size of only 355 mm^2, 27 mm^2 less than the smallest realization of Antenna I. This indicates that seemingly minor geometrical variations may significantly influence the antenna performance. (The topological differences between Antenna I and II are only in different radiator and feed line shapes; see also Fig. 4.)

Another important observation is that—for the considered structures—the size change has different impact on the reflection responses. The slope of the Pareto-optimal set obtained for the Antenna II is the highest among the compared structures. It means that the change of the reflection characteristics have limited impact on the structure size (for the Antenna II the change of F_2 along Pareto front is 30% compared to 40% for Antennas I and III). Such information is valuable, e.g., for space limited applications where small changes of antenna footprint for large variations of other objectives may be desirable. It should be reiterated that direct assessment of Pareto fronts is conclusive in terms of performance comparison of considered antennas.

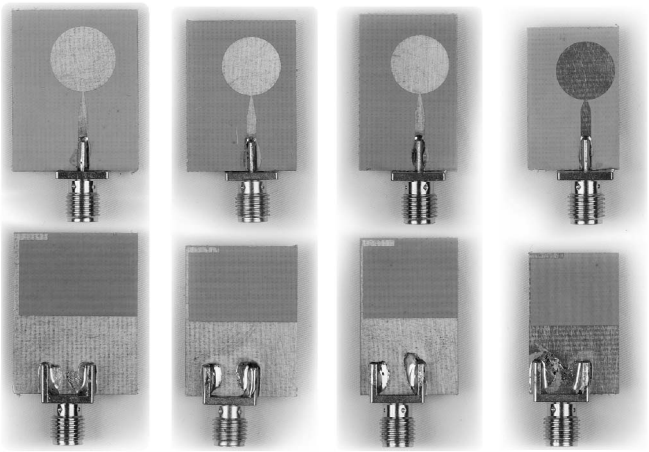

Fig. 8. Antenna I: photographs of the manufactured prototypes of the designs selected from Table I. (a) $\boldsymbol{x}_f^{(1)}$. (b) $\boldsymbol{x}_f^{(4)}$. (c) $\boldsymbol{x}_f^{(7)}$. (d) $\boldsymbol{x}_f^{(10)}$.

An even more important aspect is that in all cases, the initial designs based on the literature are dominated by the designs corresponding to the Pareto sets found for both antennas (see Fig. 4). The Pareto-optimal designs featuring in-band reflection characteristics similar to the reference structures are 290, 121, and 230 mm^2 smaller for the Antenna I, II, and III, respectively [7], [30], [31]. In other words, the designs provided in the literature are not optimal and could have been improved by applying appropriate numerical techniques. At the same time, nonoptimality of these designs (which is actually the case for majority of the designs presented in the literature) makes various comparisons involving the literature data of limited use.

D. Experimental Validation

Selected Pareto designs (i.e., $\boldsymbol{x}_f^{(1)}$, $\boldsymbol{x}_f^{(4)}$,$\boldsymbol{x}_f^{(7)}$, $\boldsymbol{x}_f^{(10)}$) of Antenna I and II have been fabricated and measured. Detailed dimensions of the chosen structures realizations can be found in Tables I and II.

Photographs of the manufactured designs of Antenna I are shown in Fig. 8, whereas the comparison of their simulated and measured reflection characteristics can be found in Fig. 9. The obtained results indicate that the measured designs fulfill the requirements upon acceptable in-band $|S_{11}|$ response. The results are in good agreement. For the selected designs, the maximum measured in-band reflection levels are -14.8, -13.5, -11.5, and -10 dB, respectively. Therefore, the peak vertical discrepancies between the simulation and measurement results are 2, 1.6, 1.4, and 0.3 dB for $\boldsymbol{x}_f^{(1)}$,$\boldsymbol{x}_f^{(4)}$,$\boldsymbol{x}_f^{(7)}$, and $\boldsymbol{x}_f^{(10)}$.

Fig. 10 shows the photographs of the fabricated Antenna II designs, whereas the comparison of their simulated and measured characteristics is shown in Fig. 11. Similarly as for previous structure, the agreement between the results is acceptable. The maximum measured in-band $|S_{11}|$ for the antenna designs are -14.4, -12.9, -11, and -9.9 dB, respectively. The peak vertical misalignment between the responses is 1 dB, 0.9, 0.5, and 0.2 dB for $\boldsymbol{x}_f^{(1)}$,$\boldsymbol{x}_f^{(4)}$,$\boldsymbol{x}_f^{(7)}$, and $\boldsymbol{x}_f^{(10)}$.

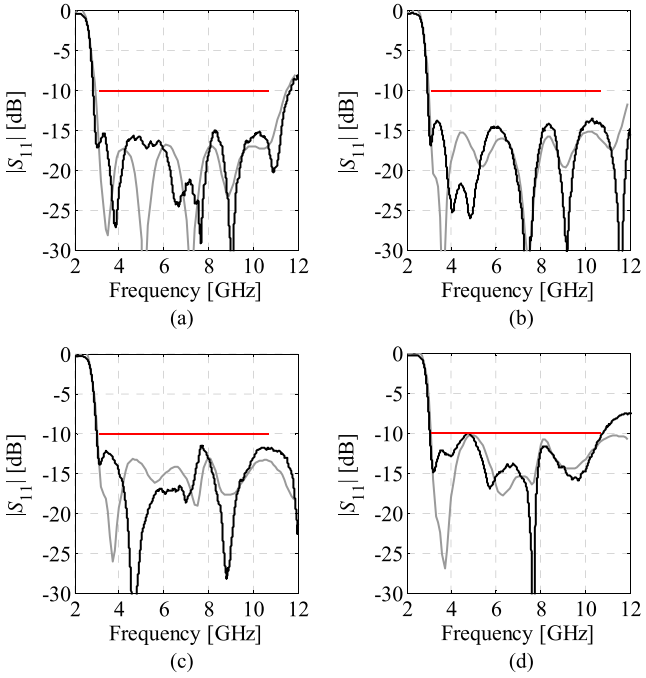

Fig. 9. Antenna I: comparison of simulated (gray line) and measured (black line) reflection characteristics obtained for the designs selected from Table I. (a) $\boldsymbol{x}_f^{(1)}$. (b) $\boldsymbol{x}_f^{(4)}$. (c) $\boldsymbol{x}_f^{(7)}$. (d) $\boldsymbol{x}_f^{(10)}$.

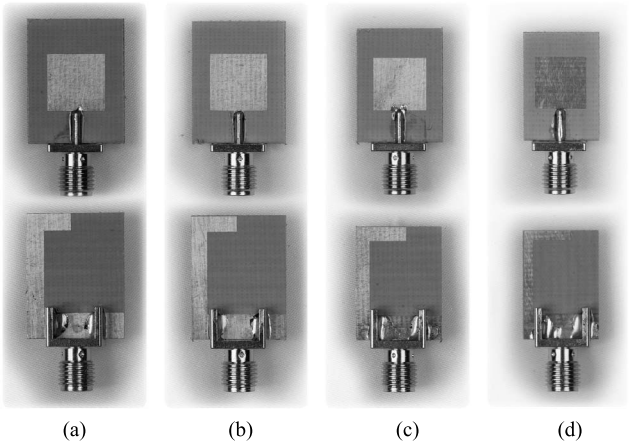

Fig. 10. Antenna II: photographs of the manufactured prototypes of the designs selected from Table II. (a) $\boldsymbol{x}_f^{(1)}$. (b) $\boldsymbol{x}_f^{(4)}$. (c) $\boldsymbol{x}_f^{(7)}$. (d) $\boldsymbol{x}_f^{(10)}$.

The simulated and measured Pareto sets obtained from both considered antenna structures are shown in Fig. 12. Although the shapes of both sets are similar, increasing vertical misalignment between antenna responses for lower reflection levels can be observed. The discrepancies between the simulated and measured responses for both antennas are due to fabrication tolerances, imperfections of the structure assembly as well as electrically large measurement setup. It should be emphasized that the considered structures are electrically small. Therefore, the aforementioned factors noticeably influence the measured responses.

V. Case Study: Three-Objective Antenna Comparison

In this section, we demonstrate antenna multiobjective-optimization-based antenna comparison involving three

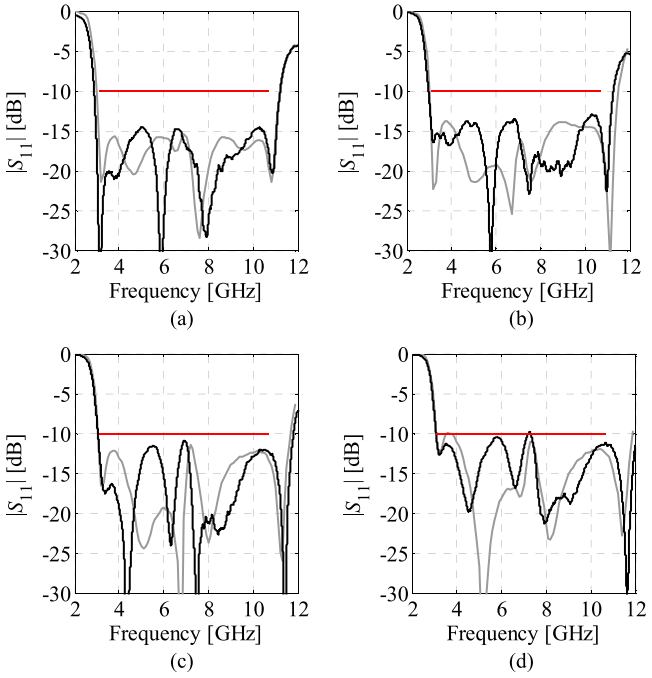

Fig. 11. Antenna II: comparison of simulated (gray line) and measured (black line) $|S_{11}|$ responses of designs selected from Table II. (a) $\boldsymbol{x}_f^{(1)}$. (b) $\boldsymbol{x}_f^{(4)}$. (c) $\boldsymbol{x}_f^{(7)}$. (d) $\boldsymbol{x}_f^{(10)}$.

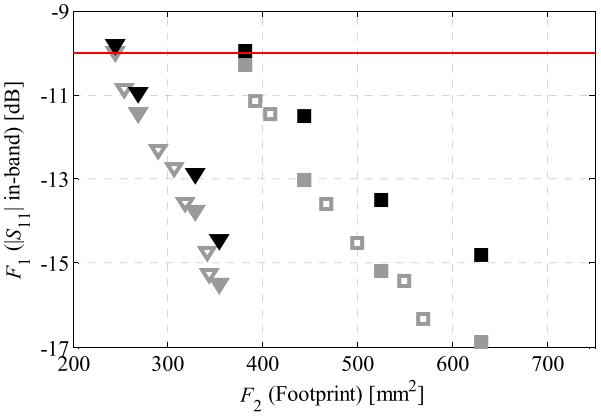

Fig. 12. Comparison of the simulated (gray symbols) and measured (black symbols) Pareto sets obtained for Antenna I (□) and Antenna II (▽). Filled markers denote designs $\boldsymbol{x}_f^{(1)}$, $\boldsymbol{x}_f^{(4)}$, $\boldsymbol{x}_f^{(7)}$, and $\boldsymbol{x}_f^{(10)}$.

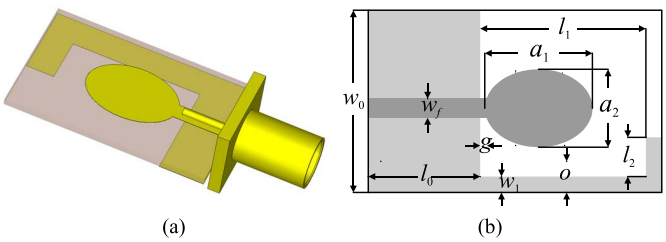

Fig. 13. Geometry of Antenna IV. (a) 3-D view. (b) Front view with geometry parameters marked.

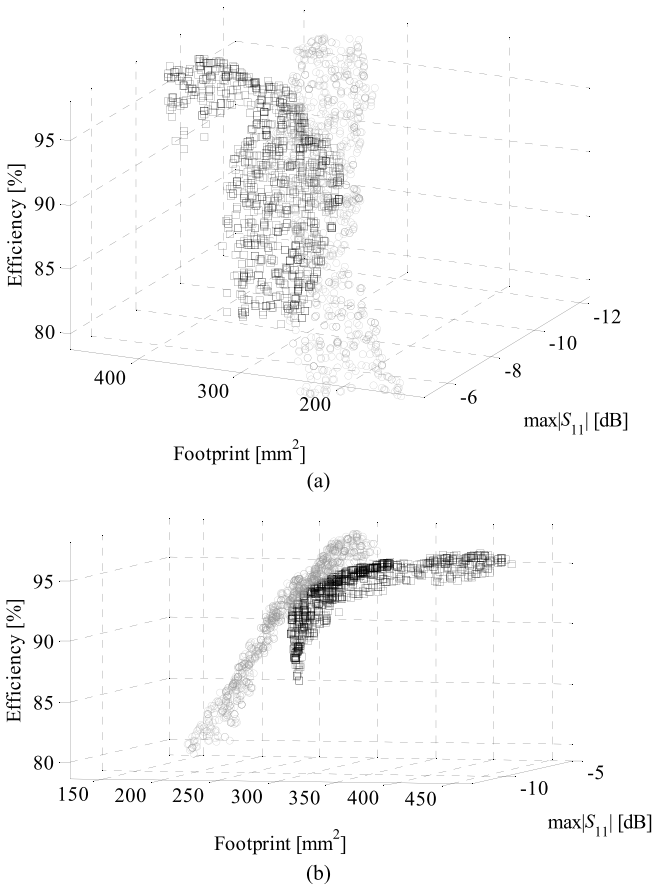

Fig. 14. Pareto fronts for Antenna II (o) and Antenna IV (□). (a) View showing the ranges of the objectives along the front. (b) View indicating that Antenna IV is entirely dominated by Antenna II.

objectives: the reflection response, and the average total efficiency in 3.1 to 10.6 GHz range, and the size. In this case, the Pareto fronts are obtained using surrogate-based optimization scheme involving three stages: 1) identification of the extreme Pareto designs [as in (1)]; 2) construction of the reliable data-driven surrogate using kriging interpolation and EM simulation data sampled in the region spanned by the extreme designs; and 3) multiobjective optimization of the surrogate using MOEA [46]. For the sake of demonstration, we compare Antenna II [see Fig. 4(b)] and Antenna IV as shown in Fig. 13. Antenna IV is a version of Antenna II where the square radiator has been replaced by the elliptical one. Also, the number of design parameters has been increased by one to $\boldsymbol{x}_{\mathrm{IV}} = [l_0\ g\ a_1\ a_2\ l_1\ l_2 w_1\ o]^T$. Computational models for both structures contain the same SMA connector, included to ensure reliability of the simulation results. The ranges of design variables for considered design are: $\boldsymbol{l}_{\mathrm{II}} = [4\ -2\ 4\ 5\ 1\ 0.5\ 0.5]^T$ and $\boldsymbol{u}_{\mathrm{II}} = [15\ 2\ 15\ 20\ 10\ 3.5\ 5.5]^T$.

The Pareto fronts for Antenna II and Antenna IV are shown in Fig. 14. It can be observed that the front of Antenna II spans much wider than the one of Antenna IV (e.g., the best maximum in-band reflection value of -12.6 dB for Antenna II and -11.5 dB for Antenna IV, and the smallest size around 115 mm^2 versus 230 mm^2 for Antenna IV at the -5 dB level). Overall, as indicated in Fig. 14(b), the front for Antenna IV is entirely dominated by that of Antenna II. The obtained results

suggests that despite lower number of degrees of freedom, rectangular radiator allows for obtaining better performance (in terms of possible design tradeoffs) than the elliptical one.

VI. Conclusion

In this paper, a methodology for comprehensive performance comparison of UWB antenna structures in terms of possible design trade-offs has been presented. The objectives of interest are the structure size and its electrical performance. For the sake of illustration, reflection characteristics (specifically, the maximum in-band reflection level), as well as antenna efficiency, are utilized as the figures of interest. Our approach exploits fast multiobjective optimization that permits identification of the Pareto set representation at the computational cost corresponding to about a hundred of EM analyses of the antenna. Comparison of the obtained Pareto sets allows for verifying antenna capabilities in terms of possible miniaturization rates as well as the best possible in-band reflection levels.

As demonstrated using three examples of compact UWB antennas, fast multiobjective optimization permits the most comprehensive and conclusive comparison of alternative antenna topologies that can be executed in reasonable timeframe. The obtained results indicate that the structures can be ordered in the sense of Pareto dominance relation with the best antenna entirely dominating the other two, and the second dominating the third one. This means, in particular, that one of the structures is the best both in terms of the minimum attainable size (while ensuring acceptable matching) and the minimum in-band reflection level. At the same time, comparison with the initial designs from the literature (clearly nonoptimal for both structures) indicates the importance of proper geometry optimization in order to ensure the best possible performance. A separate case study has been provided concerning three design objectives (size, matching, and efficiency). Clearly, increasing the number of objectives makes the design optimization (especially multiobjective one) quite challenging. Future research will be focused on considering even more comprehensive set of criteria.

For additional verification, simulation results provided in this paper have been supported by experimental data for several fabricated prototypes of selected antenna structures. The simulated and measured Pareto sets are in good agreement which is an additional evidence to confirm the usefulness of the method.

Acknowledgment

The authors would like to thank Computer Simulation Technology AG, Darmstadt, Germany, for making CST Microwave Studio available.

References

[1] M. Bod, H. R. Hassani, and M. M. S. Taheri, "Compact UWB printed slot antenna with extra bluetooth, GSM, and GPS bands," *IEEE Antennas Wireless Propag. Lett.*, vol. 11, pp. 531–534, 2012.

[2] P. B. Samal, P. J. Soh, and G. A. E. Vandenbosch, "UWB all-textile antenna with full ground plane for off-body WBAN communications," *IEEE Trans. Antennas Propag.*, vol. 62, no. 1, pp. 102–108, Jan. 2014.

[3] H. R. Khaleel, H. M. Al-Rizzo, D. G. Rucker, and S. Mohan, "A compact polyimide-based UWB antenna for flexible electronics," *IEEE Antennas Wireless Propag. Lett.*, vol. 11, pp. 564–567, 2012.

[4] S. Zhang, B. K. Lau, A. Sunesson, and S. He, "Closely-packed UWB MIMO/diversity antenna with different patterns and polarizations for USB dongle applications," *IEEE Trans. Antennas Propag.*, vol. 60, no. 9, pp. 4372–4380, Sep. 2012.

[5] H. Ning, *Unit and Ubiquitous Internet of Things*. Boca Raton, FL, USA: CRC Press, 2013.

[6] L. Lizzi and F. Ferrero, "Use of ultra-narrow band miniature antennas for Internet-of-Things applications," *Electron. Lett.*, vol. 51, no. 24, pp. 1964–1966, 2015.

[7] N. Chahat, M. Zhadobov, R. Sauleau, and K. Ito, "A compact UWB antenna for on-body applications," *IEEE Trans. Antennas Propag.*, vol. 59, no. 4, pp. 1123–1131, Apr. 2011.

[8] A. Bekasiewicz and S. Koziel, "Structure and design optimisation of compact UWB slot antenna," *Electron. Lett.*, vol. 52, no. 9, pp. 681–682, 2016.

[9] C. A. Balanis, *Antenna Theory Analysis and Design*, 3rd ed. Hoboken, NJ, USA: Wiley, 2005.

[10] S. Koziel and A. Bekasiewicz, "A structure and simulation-driven design of compact CPW-fed UWB antenna," *IEEE Antennas Wireless Propag. Lett.*, vol. 15, pp. 750–753, 2016.

[11] L. Liu, S. W. Cheung, and T. I. Yuk, "Compact MIMO antenna for portable devices in UWB applications," *IEEE Trans. Antennas Propag.*, vol. 61, no. 8, pp. 4257–4264, Aug. 2013.

[12] A. Bekasiewicz and S. Koziel, "Structure and computationally efficient simulation-driven design of compact UWB monopole antenna," *IEEE Antennas Wireless Propag. Lett.*, vol. 14, pp. 1282–1285, 2015.

[13] J.-F. Li, Q.-X. Chu, Z.-H. Li, and X.-X. Xia, "Compact dual band-notched UWB MIMO antenna with high isolation," *IEEE Trans. Antennas Propag.*, vol. 61, no. 9, pp. 4759–4766, Sep. 2013.

[14] Y.-F. Liu, P. Wang, and H. Qin, "Compact ACS-fed UWB monopole antenna with extra Bluetooth band," *Electron. Lett.*, vol. 50, no. 18, pp. 1263–1264, 2014.

[15] T. K. Roshna, U. Deepak, V. R. Sajitha, and P. Mohanan, "Coplanar stripline-fed compact UWB antenna," *Electron. Lett.*, vol. 50, no. 17, pp. 1181–1182, Aug. 2014.

[16] L. Guo, S. Wang, X. Chen, and C. G. Parini, "Study of compact antenna for UWB applications," *Electron. Lett.*, vol. 46, no. 2, pp. 115–116, 2010.

[17] L. Guo, S. Wang, X. Chen, and C. Parini, "A small printed quasi-self-complementary antenna for ultrawideband systems," *IEEE Antennas Wireless Propag. Lett.*, vol. 8, pp. 554–557, 2009.

[18] C.-Y. Huang and J.-Y. Su, "A printed band-notched UWB antenna using quasi-self-complementary structure," *IEEE Antennas Wireless Propag. Lett.*, vol. 10, pp. 1151–1153, 2011.

[19] W.-T. Chung, and C.-H. Lee, "Compact slot antenna for UWB applications," *IEEE Antennas Wireless Propag. Lett.*, vol. 9, pp. 63–66, 2010.

[20] M. Gopikrishna, D. D. Krishna, C. K. Aanandan, P. Mohanan, and K. Vasudevan, "Design of a microstip fed step slot antenna for UWB communication," *Microw. Opt. Technol. Lett.*, vol. 51, no. 4, pp. 1126–1129, 2009.

[21] J. Nocedal and S. Wright, *Numerical Optimization*, 2nd ed. New York, NY, USA: Springer, 2006.

[22] A. R. Conn, K. Scheinberg, and L. N. Vincente, *Introduction to Derivative-Free Optimization*. Philadelphia, PA, USA: SIAM, 2009.

[23] S. Koziel and S. Ogurtsov, *Antenna Design by Simulation-Driven Optimization. Surrogate-Based Approach*. New York, NY, USA: Springer, 2014.

[24] S. Koziel, X. S. Yang, and Q. J. Zhang, Eds., *Simulation-Driven Design Optimization and Modeling for Microwave Engineering*. London, U.K.: Imperial College Press, 2013.

[25] M. B. Yelten, T. Zhu, S. Koziel, P. D. Franzon, and M. B. Steer, "Demystifying surrogate modeling for circuits and systems," *IEEE Circuits Syst. Mag.*, vol. 12, no. 1, pp. 45–63, 1st Quart., 2012.

[26] S. Koziel and J. W. Bandler, "Rapid yield estimation and optimization of microwave structures exploiting feature-based statistical analysis," *IEEE Trans. Microw. Theory Techn.*, vol. 63, no. 1, pp. 107–114, Jan. 2015.

[27] M. A. E. Sabbagh, M. H. Bakr, and J. W. Bandler, "Adjoint higher order sensitivities for fast full-wave optimization of microwave filters," *IEEE Trans. Microw. Theory Techn.*, vol. 54, no. 8, pp. 3339–3351, Aug. 2006.

[28] M. Ghassemi, M. Bakr, and N. Sangary, "Antenna design exploiting adjoint sensitivity-based geometry evolution," *IET Microw. Antennas Propag.*, vol. 7, no. 4, pp. 268–276, 2013.
[29] S. Koziel and A. Bekasiewicz, "Fast EM-driven size reduction of antenna structures by means of adjoint sensitivities and trust regions," *IEEE Antennas Wireless Propag. Lett.*, vol. 14, pp. 1681–1684, 2015.
[30] T. Li, H. Zhai, G. Li, L. Li, and C. Liang, "Compact UWB band-notched antenna design using interdigital capacitance loading loop resonator," *IEEE Antennas Wireless Propag. Lett.*, vol. 11, pp. 724–727, 2012.
[31] X. Qing and Z. N. Chen, "Compact coplanar waveguide-fed ultra-wideband monopole-like slot antenna," *IET Microw. Antennas Propag.*, vol. 3, no. 5, pp. 889–898, 2009.
[32] S. Koziel and A. Bekasiewicz, "Multiobjective antenna design by means of sequential domain patching," *IEEE Antennas Wireless Propag. Lett.*, vol. 15, pp. 1089–1092, 2015.
[33] H. Choo, R. L. Rogers, and H. Ling, "Design of electrically small wire antennas using a Pareto genetic algorithm," *IEEE Trans. Antennas Propag.*, vol. 53, no. 3, pp. 1038–1046, Mar. 2005.
[34] S. Koulouridis, D. Psychoudakis, and J. L. Volakis, "Multiobjective optimal antenna design based on volumetric material optimization," *IEEE Trans. Antennas Propag.*, vol. 55, no. 3, pp. 594–603, Mar. 2007.
[35] K. Deb, *Multi-Objective Optimization Using Evolutionary Algorithms*. New York, NY, USA: Wiley, 2001.
[36] S. Chamaani, M. S. Abrishamian, and S. A. Mirtaheri, "Time-domain design of UWB Vivaldi antenna array using multiobjective particle swarm optimization," *IEEE Antennas Wireless Propag. Lett.*, vol. 9, pp. 666–669, 2010.
[37] Y. Kuwahara, "Multiobjective optimization design of Yagi-Uda antenna," *IEEE Trans. Antennas Propag.*, vol. 53, no. 6, pp. 1984–1992, Jun. 2005.
[38] C.-C. Lin, S.-W. Kuo, and H.-R. Chuang, "A 2.4-GHz printed meander-line antenna for USB WLAN with notebook-PC housing," *IEEE Microw. Wireless Compon. Lett.*, vol. 15, no. 9, pp. 546–548, Sep. 2005.
[39] S. Koziel and S. Ogurtsov, "Multi-objective design of antennas using variable-fidelity simulations and surrogate models," *IEEE Trans. Antennas Propag.*, vol. 61, no. 12, pp. 5931–5939, Dec. 2013.
[40] S. Koziel and A. Bekasiewicz, "Rapid multiobjective antenna design using point-by-point Pareto set identification and local surrogate models," *IEEE Trans. Antennas Propag.*, vol. 64, no. 6, pp. 2551–2556, Jun. 2016.
[41] S. Koziel, "Computationally efficient multi-fidelity multi-grid design optimization of microwave structures," *Appl. Comput. Electromagn. Soc. J.*, vol. 25, no. 7, pp. 578–586, 2010.
[42] A. I. J. Forrester and A. J. Keane, "Recent advances in surrogate-based optimization," *Prog. Aerosp. Sci.*, vol. 45, pp. 50–79, Jan./Apr. 2009.
[43] S. Koziel, A. Bekasiewicz, and W. Zieniutycz, "Expedited EM-driven multiobjective antenna design in highly dimensional parameter spaces," *IEEE Antennas Wireless Propag. Lett.*, vol. 13, pp. 631–634, 2014.
[44] S. Koziel and A. Bekasiewicz, "Low-cost multi-objective optimization of antennas using Pareto front exploration and response features," in *Proc. IEEE Int. Symp. Antennas Propag.*, Fajardo, Puerto Rico, Jun. 2016, pp. 571–572.
[45] CST Microwave Studio, CST AG, Darmstadt, Germany, 2015. [Online]. Available: http://www.cst.com
[46] A. Bekasiewicz, S. Koziel, W. Zieniutycz, and L. Leifsson, "Expedited simulation-driven multi-objective design optimization of quasi-isotropic dielectric resonator antenna," in *Simulation-Driven Modeling and Optimization*. New York, NY, USA: Springer, 2016, pp. 207–231.

Slawomir Koziel (M'03–SM'07) received the M.Sc. and Ph.D. degrees in electronic engineering from the Gdansk University of Technology, Gdansk, Poland, in 1995 and 2000, respectively, and the M.Sc. degrees in theoretical physics and mathematics and the Ph.D. degree in mathematics from the University of Gdansk, Gdansk, Poland, in 2000, 2002, and 2003, respectively.

He is currently a Professor with the School of Science and Engineering, Reykjavik University, Reykjavik, Iceland. He is also a Visiting Professor with the Gdansk University of Technology His current research interests include CAD and modeling of microwave circuits, simulation-driven design, surrogate-based optimization, space mapping, circuit theory, analog signal processing, evolutionary computation, and numerical analysis.

Adrian Bekasiewicz received the M.Sc. and Ph.D. degrees in electronic engineering from the Gdansk University of Technology, Gdansk, Poland, in 2011 and 2016, respectively.

He is currently a Post-Doctoral Fellow with the School of Science and Engineering, Reykjavik University, Reykjavik, Iceland. He is also a Researcher with Gdansk University of Technology. His current research interests include EM-driven design, multiobjective optimization, metaheuristic algorithms, development of compact antennas, and miniaturization of microwave/RF components.